Acta Crystallographica Section A
Foundations of Crystallography
ISSN 0108-7673

Received 6 November 2006
Accepted 22 December 2006

Ab initio neutron crystallography by the charge flipping method

Gábor Oszlányi* and András Sütő

Research Institute for Solid State Physics and Optics of the Hungarian Academy of Sciences, POB 49, H-1525 Budapest, Hungary. Correspondence e-mail: go@szfki.hu

In this paper, the charge flipping method is proposed for *ab initio* structure determination using neutron diffraction data alone. For this purpose, a new variant of the dual-space iterative algorithm is introduced, which is called *band flipping*. Unlike the basic algorithm, it reverses the sign of scattering density only within a zero-centred band, develops large plateaus without forcing positivity, and often leads to Babinet solutions. Its phasing power was tested on two organic structures. These behave similarly when using X-ray diffraction data and the basic algorithm but, with neutron data and band flipping, their solution becomes orders-of-magnitude more difficult and strongly dependent on the hydrogen content. Surprisingly, when the constraint of positivity is added, convergence speeds up to the point where structure determination using neutron diffraction data is not more difficult than the X-ray case. However, by following the evolution of the *R* factor, such a solution can be easily missed, and band flipping must be used both as a probe of convergence and as a tool for developing negative densities. Apart from demonstrating the feasibility of charge flipping for *ab initio* neutron crystallography, the present study also leads to an important byproduct: the type of traps that occasionally block the iterative process are identified and a mathematical analysis of their origin is given.

1. Introduction

The speed and availability of fast Fourier transform (FFT) codes (Brigham, 1974; Frigo & Johnson, 1998) and the increase in desktop computing power are changing the way modern direct methods can approach the phase problem of crystallography. Two recent examples for the structure determination of undersampled periodic objects are the difference map (DM) and the charge flipping (CF) algorithms (Elser, 2003; Oszlányi & Sütő, 2004, 2005). These methods are strongly related to the pioneering work of Gerchberg, Saxton and Fienup on non-periodic objects in optics (Gerchberg & Saxton, 1972; Fienup, 1982) and to density modification in protein crystallography (Wang, 1985; Shiono & Woolfson 1992; Abrahams & Leslie, 1996; Zhang *et al.*, 2001). The dual-space iterative character of all these methods makes them somewhat similar, but there are also a number of critical algorithmic details that differ. At present, DM and CF algorithms are not competitive with more complex multi-strategy program packages such as *SHELX*, *SIR* or *SnB* (Sheldrick, 1997; Burla *et al.*, 2005; Miller *et al.*, 1993), but with an increasing number of useful applications they can already serve as complementary tools.

In this paper, we focus on the role of constraints in solving the phase problem by the CF method (Oszlányi & Sütő, 2004, 2005). Recall that a truly *ab initio* case of structure solution means the presence of real scattering density, the use of a single non-anomalous data set up to high resolution and no preliminary information on absolute scale, chemical composition, atom types or crystal symmetry. In this case, any set of unknown phases is perfectly compatible with the measured structure-factor moduli, and it is only the use of constraints that will select the correct solution in the high-dimensional phase space. Classical direct methods rely on the two very efficient constraints of positivity and atomicity, both expressed as statistical phase relations in reciprocal space. A dual-space iterative process, such as charge flipping, has some more direct options to prescribe properties of the scattering density in real space. The observation that the electron density of the unit cell is mostly empty even leads to a new type of constraint, we call these *plateaus*, *i.e.* extended electron-density regions with a nearly constant value. The presence of zero-valued plateaus – seen as small ripples with high-resolution data – is not identical to atomicity and its use as a loose constraint seems to be less efficient at first glance. However, it works remarkably well in practice for periodic single crystals (Wu *et al.*, 2004; Oszlányi *et al.*, 2006) and even powders (Wu *et al.*, 2006; Baerlocher *et al.*, 2006, 2007). Its application in superspace has also provided a method of structure solution for modulated structures and quasicrystals (Palatinus, 2004; Zúñiga *et al.*, 2006; Palatinus *et al.*, 2006; Katrych *et al.*, 2007). This is a significant achievement because the field of aperiodic structures cannot utilize three-dimensional atomicity, and for some time it has badly needed a general single-pass method for

structure solution. In previous publications, the constraint of plateaus was always coupled with positivity, which is a natural combination with X-ray diffraction data. Here we shall study the phasing power of plateaus alone, which could open the way towards *ab initio* neutron crystallography.

The plan of the paper is as follows. First we shall briefly describe the basic CF algorithm, then consider artificial and physical cases of negative scattering density and define the band version of the CF algorithm to treat the negative scattering density of some atom types in neutron diffraction. Later, we select two similar organic structures with medium and high hydrogen content, and evaluate the algorithm variants for these test structures. Our main conclusion is that a substantial contribution of negative density does still allow structure determination by flipping charge in a band, and by opening up the space of negative scattering density we easily see the Babinet solutions. However, it comes as a surprise that adding the constraint of positivity can speed up the convergence by orders of magnitude, but such a solution can be easily missed without the use of the band CF as a probe. For the first time, we also identify the traps that occasionally block the iterative process and present a mathematical analysis of their possible origin. Initially, these results were thought to be only of theoretical interest but, with more intense new neutron sources in sight, it is likely that *ab inito* structure solution by using neutron diffraction data alone will become more widespread in practice. At least, here is one more algorithm to help this happen.

2. The basic charge flipping algorithm

The charge flipping algorithm is an iterative Fourier recycling scheme that has been described in detail in our two recent papers (Oszlányi & Sütő, 2004, 2005). The first introduces the basic CF algorithm with the name-giving modification of low electron density in real space, while the second defines a very efficient version of the same scheme that complements the exploration of phases by a perturbation of weak reflections in reciprocal space. In the following, we shall summarize and apply only the basic version of CF.

$$\begin{array}{ccc} \rho & \xrightarrow{\text{FLIP}} & g \\ {\scriptstyle \text{FFT}^{-1}}\uparrow & & \downarrow{\scriptstyle \text{FFT}} \\ F & \xleftarrow[\text{DATA}]{} & G \end{array} \qquad (1)$$

Equation (1) shows one iteration cycle of the basic CF algorithm. It requires high-resolution data within the resolution sphere ($d_{\min} \sim 0.8$ Å) and the electron density represented on a sufficiently fine grid ($\Delta r < d_{\min}/2$). (However, with simple structures or by estimating the intensity of reflections beyond the sphere, this resolution requirement may be too strict and can be significantly relaxed.) For initialization, $F(0)$ is set to zero, and a random phase set is selected that satisfies Friedel's law $\varphi(-\mathbf{h}) = -\varphi(\mathbf{h})$. Then structure factors are created as $F(\mathbf{h}) = F_{\text{obs}}(\mathbf{h}) \exp[i\varphi(\mathbf{h})]$ and the electron density is calculated by the inverse FFT. This $\rho(\mathbf{r})$ is the starting point of the iteration cycle in real space. The first modification creates a temporary electron density $g(\mathbf{r})$ by changing (flipping) the sign of $\rho(\mathbf{r})$ if it falls below a threshold δ and leaving it unchanged otherwise. The *positive* δ is the only parameter of the algorithm, its optimal value is a few percent of the maximum electron density. In the next step, temporary structure factors $G(\mathbf{h})$ are calculated by the FFT. These complex structure factors are then modified in different ways to obtain the next approximation of $F(\mathbf{h})$. For observed reflections, the phases are kept and the calculated moduli are replaced by the observed ones. Reflections outside the resolution sphere are reset to zero, while the forward scattering, corresponding to the total charge, is accepted as is, $F(0) = G(0)$. Finally, the iteration cycle is completed by an inverse FFT and a new $\rho(\mathbf{r})$. This iteration process can continue unconditionally, the R factor serves only for monitoring the progress. Convergence is indicated by a sharp drop in R and at this point the iteration can be stopped.

It is obvious that, while the reciprocal half of the basic algorithm simply prescribes the observed data, for the exploration of phases the real-space flipping operation is essential. The high-dimensional phase space can be viewed as a dynamical system, where the algorithm defines the dynamics that drives a given $\{\varphi(\mathbf{h})\}$ phase set as a point around. The flipping operation is part of the dynamics, and acts as a perturbation that simultaneously develops both positivity and zero plateaus. It is important to note that, while the whole process is deterministic, far from the solution it is also strongly chaotic, the iteration path is extremely sensitive to the slightest change of the starting or intermediate phases. With some patience, the path can fall within the convergence region of the solution, where the synchronization of phases occurs quickly as a phase transition. The solution to be found is itself degenerate and the degeneracy is determined by both trivial symmetries of the diffraction data (*i.e.* shift, spatial inversion and sign reversal of the scattering density) and space-group symmetries of the crystal. Once such a solution is hit, it is very stable against deterministic or random perturbations, including the dynamics that has driven the phase set into this state. The resulting structural model is also rather complete and can easily be refined by standard least-squares programs. As an even better approach, the electron density itself can be refined by the program *EDEN* (Szöke, 1993, 2006) and the atomic model can be created only afterwards.

Here we briefly summarize the main characteristics of the CF method. The first is its extreme simplicity and easy implementation. The second is its truly *ab initio* character. The electron density is represented on a grid but the concept of atoms is not acknowledged during the solution. Therefore, CF makes no use of atom types, chemical composition or even the total charge of the unit cell. There is no utilization of symmetries either, all structures are allowed to float freely in the space group $P1$. This means that the content of the whole unit cell must be determined and not only that of the asymmetric unit. The principle of such an algorithm differs a great deal from that of both classical direct methods and global optimization, it works without statistical phase relations or by using any figure of merit as a cost function. Therefore, charge

flipping is complementary to other direct methods, it can work well in troublesome situations such as the presence of pseudosymmetry or disorder. For the present work, it is also important that in the basic CF algorithm the constraints of positivity and plateaus are always coupled – in the following we shall decouple these.

3. Negative scattering density

Before we try to handle negative scattering density, we must make a clear distinction between its artificial and physical forms. Artificial negative density is caused by resolution cut-off and would disappear with infinitely high resolution data. In X-ray diffraction, it occurs by the use of both unnormalized $F(\mathbf{h})$ or normalized $E(\mathbf{h})$ structure factors, the latter leading to higher positive peaks and an enhanced negative part. In contrast, physical negative density comes from the contribution of some nuclei in neutron diffraction and would also persist with infinite resolution data. Natural abundances of the elements H, Li, Mn and Ti are the few examples that scatter out of phase with the rest of the Periodic Table, without their presence the original charge flipping algorithm would be adequate also for neutron crystallography.

For a typical organic structure (example I of the following tests), all three cases of negative density are shown in Fig. 1. In these calculations, we first generated the ideal structure factors up to 0.8 Å resolution, the isotropic displacement parameter was set to zero. For normal X-ray and neutron data, we used the corresponding atomic form factors and neutron scattering lengths, while ideal E's were calculated using point atoms instead of the usual approximate normalization. Then a Fourier inversion provided the finite resolution representation of the scattering density on a 0.33 Å grid and, finally, these volume samples were sorted and plotted in ascending order. Even if X-ray and neutron calculations are on a different scale, it is obvious that negative density is present in the increasing order: X-ray F < X-ray E < neutron data. The basic CF algorithm was not devised to handle negative density, so this increase is expected to cause a serious problem. When the positive maximum of all curves are scaled together, we can notice another region that may affect how a given scattering-density distribution responds to a given algorithm. This is the region of positive upturn. A sharper upturn – as in the case of normalized structure factors – means a smaller number of large positive pixels and, hopefully, a smaller search space to find the solution.

Considering that most direct methods operate with E's instead of F's, it is a natural question whether their use leads to faster convergence also with the charge flipping algorithm. We can confirm that this is indeed the cased. A detailed study would be a sidetrack here, but some convincing observations are listed. For example, if we take the hard-to-solve test structure of our second paper [CSD code `gidjae` (Karle *et al.*, 1987)] and a statistic of 100 runs of the basic CF algorithm, the use of E's is worth a 20-fold speed up with an optimal δ parameter. In other cases, this factor can be less and it also depends on structural features. As an extreme, for regular centrosymmetric crystals (like the test structures of the present paper), we may experience no significant speed up, but these are the cases that are easily solved already by the basic CF algorithm. We conclude that sharpening is done for its positive effect; in the act of increasing the large positive electron density, it actually decreases the effective dimensionality of the problem. Unfortunately, at the same time, it also amplifies the artificial negative part of the scattering-density distribution. At each charge flipping cycle, large negative samples must change their sign, which is unnecessary and can be harmful. The two effects of using E's are always coupled. Obviously, with X-ray diffraction data at high resolution, the positive effect dominates and the only harm is the smaller drop in the R factor at convergence. Finally, we emphasize that the speed up experienced by the use of E's also applies for the higher efficiency $\pi/2$ version of the CF algorithm (Oszlányi & Sütő, 2005). So for the solution of complex structures, we can already utilize two independent (order-of-magnitude) improvements that are additive!

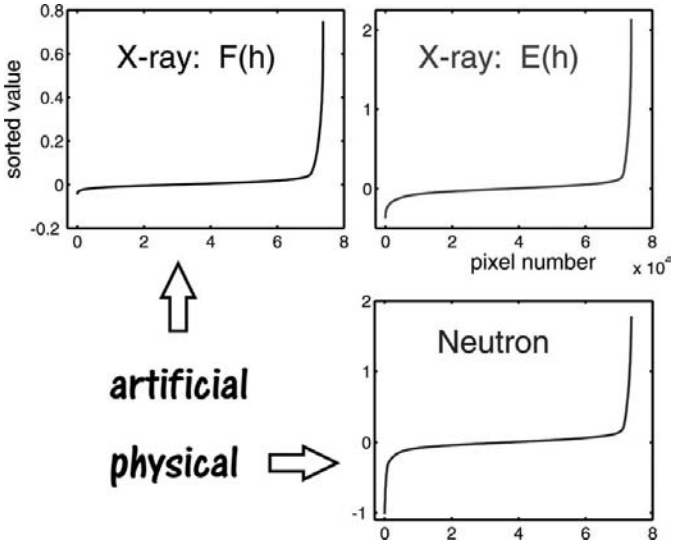

Figure 1
Scattering density of a typical organic structure (example I) represented on a 0.33 Å grid, pixels are sorted in ascending order. The three separate subplots show artificial and physical cases of negative density calculated by using X-ray F, X-ray E and neutron data at 0.8 Å resolution.

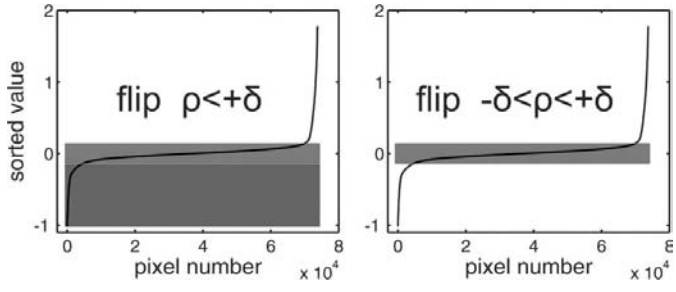

Figure 2
Scattering density of a typical organic structure (example I) represented on a grid, pixels are sorted in ascending order. Left and right panels show the different flipping regions of the basic and band CF algorithms.

4. Band charge flipping

Now let us return to the case of physical negative density that will surely require a new algorithm. The simplest approach is to modify only the $\rho \rightarrow g$ step of the basic iteration cycle and reverse the sign of the scattering density only within a fixed $[-\delta, +\delta]$ band. For a graphical comparison, Fig. 2 shows the sorted scattering density samples of our first test structure and the regions that are flipped by the basic and the band CF algorithms. Band charge flipping had always been considered as one of many algorithm variants, but as it relies only on the constraint of plateaus it was found to be less efficient for X-ray data than other versions that utilize positivity. However, without positivity of the scattering density itself, such an algorithm seems to be a natural choice, and its use has to be reconsidered.

At the same time, we must realize that band CF is a symmetric procedure, and from now on nothing fixes the sign of the solution. Sign reversal of the scattering density is a trivial symmetry of the diffraction data, the only difference between the structure factors corresponding to $+\rho$ and $-\rho$ is the unobserved value of $F(0)$. This ambiguity is well known in optics and the occurrence of these so-called Babinet solutions (Marks, 1999; Gilmore, 2000) is also expected in *ab initio* neutron crystallography, especially when the total charge is not used as a constraint. Furthermore, by opening up the space for negative scattering density, a situation may emerge when the contribution of false positive and negative densities add in a way that blocks the progress of the iteration. A study and analysis of these traps will be given later.

5. Test structures and runs

For a fair comparison of algorithm variants, we have selected two very similar organic structures. Of course, a large number of other alternatives was also tested, and the criterion for selecting the two examples was not the maximum size but to find a pair that makes the main point of the paper clear. The most important parameters of the test structures are given in Table 1. The two structures crystallize in the same common space group, have a similar unit-cell volume and possess a short b axis that is an advantage for graphical representation. The main difference is their hydrogen content, which can be considered as medium and high. In the neutron diffraction literature, the fraction of negative scattering is defined as $Q = 100 \sum b_H^2 / \sum b_i^2$ and the 27% value of example II is near the limit of solvability experienced by other direct methods. For the following tests, the amplitudes of X-ray and neutron structure factors were generated up to 0.8 Å resolution, the isotropic displacement parameter was set to zero and the scattering density was represented on a real-space grid with 0.33 Å spacing. We already know that the charge flipping algorithm tolerates well both noisy data and missing weak reflections, the latter can even lead to a speed up of convergence. Data completeness at large d spacing is another question and can be a problem with experiments performed at some spallation sources. So here we assume perfect data and that the amplitudes of these strong envelope-defining reflections were observed.

Table 1
Parameters of the two test structures.

Columns: CSD code and original reference, space group, unit-cell volume, chemical composition, fraction of negative scattering.

	Code and ref.	Space group	V (Å^3)	Composition	Q (%)
Example I	caxhis01 (*a*)	$P2_1/c$	2554.8	$4C_{34}H_{26}O_4$	18.2
Example II	diglou (*b*)	$P2_1/c$	2418.9	$4C_{27}H_{36}N_2$	26.9

References: (*a*) Becker *et al.* (1982); (*b*) Arduengo *et al.* (1999).

The evolution of a single run can be followed by the R factor, the total charge or the phase change and all three quantities show a sharp drop at the point of convergence. We prefer the use of the R factor for two reasons. First, it shows a very short (∼5–10 cycles) transient that can give some hint on the correct selection of the δ parameter. The ideal transient shows a modest decrease of the R factor, a too large decrease or an increase requires a larger or a smaller δ, respectively. Second, usually a rather featureless stagnation period follows, in which, apart from small fluctuations, the R factor is nearly constant. This flatness can be easily utilized to automate the recognition of the drop occurring at the convergence. The behaviour of the phase change is very similar to that of R, but it comes from an expensive calculation in every second iteration cycle that is a waste of time. Finally, the total charge is a very interesting quantity and is available without further calculation but in the stagnation period its value continuously creeps downwards, which makes it less well suited for automatic recognition of the solution. In the literature, some remarks appeared regarding the absence of a stagnation period (Wu *et al.*, 2004). We confirm that this can occur with an easy-to-solve structure and an optimal δ parameter. It means nothing else than the accidental selection of a starting phase set that already falls within the convergence region. However, in general the stagnation period is present and is an important part of the iteration process.

The phasing power of different algorithms can be evaluated and compared only on the basis of statistics. Therefore, for all subsequent work, we have selected 100 random phase sets and allowed 5000 iteration cycles for each run. The efficiency is usually measured by two numbers, the success rate and the number of iteration cycles up to convergence averaged over the successful runs. In Appendix A, we also define a single indicator, the *number of iterations spent for a solution* that is used when the success rate is less than 100%. It can be computed by choosing the maximum number of iterations smaller and, thus, its use saves computer time.

The first set of runs using unnormalized X-ray data and the basic CF algorithm should be considered as the point of reference. The evolution of the R factor is shown in Fig. 3, upper and lower panels correspond to examples I and II, while the plots from left to right correspond to an increasing value of the threshold parameter. (A range of parameters was examined, the plots are just a selection.) In both cases, the success

rate is 100% for a wide range of δ, and with its optimal choice the average number of iterations can be as small as 30 and 45 for examples I and II, respectively. This shows that the regular centrosymmetric character of the two test structures is an easy exercise for the basic algorithm.

The second set of runs was done using X-ray data and band charge flipping. Without presenting a large number of further plots, we can state the main observations. As expected, the performance of band CF is inferior to the basic algorithm. The range of δ that gives 100% success rate is narrower, and even with the best choice of δ the average number of necessary iterations goes up to 130 and 350 for examples I and II, respectively. These numbers well illustrate that there is no point of not utilizing positivity if the scattering density has this property. For both sets of X-ray studies, one might naively assume that the number of non-H atoms (152/116) is a relevant parameter that determines the difficulty of the solution. As we see here, other structural features are more important, in fact, the solution of example II with fewer non-H atoms takes more iterations for both algorithm variants.

The third set of runs was done using neutron diffraction data and the band CF algorithm. Fig. 4 shows the evolution of the *R* factor, subplots are arranged as in Fig. 3. Note that the plot range of the iteration cycles was increased by a factor of ten, and even with the best δ, shown on the right, the success rate is less than 100%. For examples I and II, the success rates are 95 and 53%, and the numbers of iterations spent for a solution are 400 and 5400, respectively. These numbers show clearly that solving the neutron case is 13 and 120 times harder than solving the basic X-ray case. Comparing the two examples, we can also check the effect of hydrogen content. For the neutron case, the total number of atoms is very similar (256/260) and the number of H atoms (104/144) that yield the negative scattering density seems to have a marked effect on the number of iterations required. Up to this point, nothing is unexpected. Band charge flipping works for neutron data, the larger number of atoms to be determined means that *ab initio* neutron crystallography is much more difficult than the X-ray case, and the larger number of H atoms further increases this difficulty. In addition, we can easily see that the scattering density of the solution is either positive or negative – these are the expected Babinet solutions.

At this point of using neutron data, we switch back to the constraint of positivity, which seems to be an odd idea considering the large negative scattering density of our test structures. The runs shown in Fig. 5 are actually combinations of the basic and band CF algorithms, the exact protocol followed was to run the basic algorithm for 500 iteration cycles and then switch to the band version for another 100 cycles. As before, upper and lower panels correspond to examples I and II, while the subplots from left to right correspond to an increasing value of the threshold parameter. There are a number of surprises in these plots. First, the magnitude of the sudden change of the *R* factor in the basic 500 cycles is much smaller than in any of the previous studies. Second, this sudden change is not always a drop: with a large δ it is, with a small δ it is a step upwards, while in between there might be nothing to be recognized. Third, any sudden change in this period corresponds to the convergence, but the iteration process might have converged even without the presence of

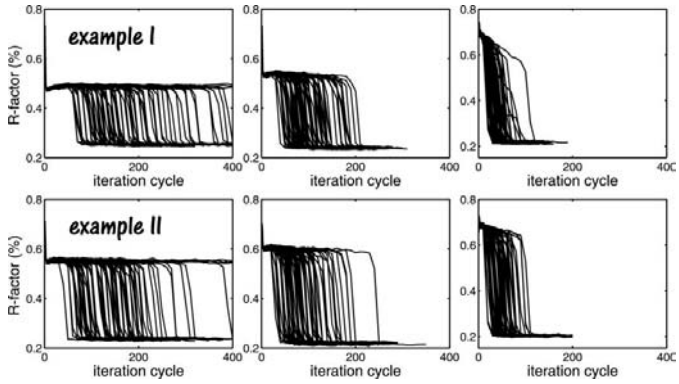

Figure 3
6×100 runs of using unnormalized X-ray data and the basic CF algorithm. Upper and lower panels correspond to test structures I and II, while plots from left to right correspond to an increasing value of the δ parameter.

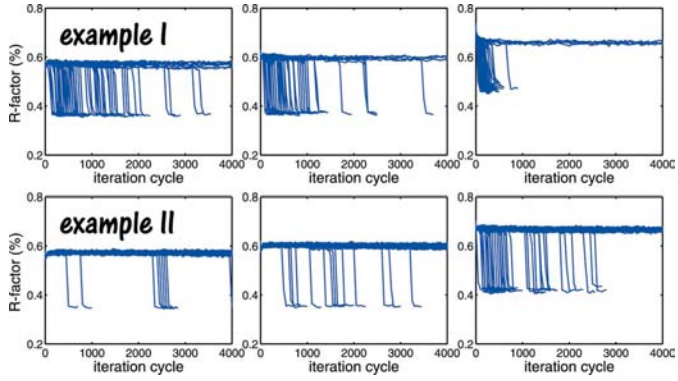

Figure 4
6×100 runs of using neutron diffraction data and the band CF algorithm. Upper and lower panels correspond to test structures I and II, while plots from left to right correspond to an increasing value of the δ parameter.

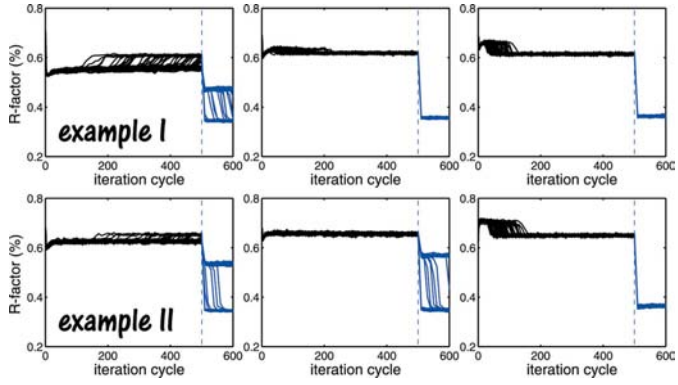

Figure 5
6×100 runs of using neutron diffraction data and a combination of the 'basic + band' CF algorithms. Upper and lower panels correspond to test structures I and II, while plots from left to right correspond to an increasing value of the δ parameter.

such a sudden change. So what is the use of the last 100 iteration cycles? Here band charge flipping allows the development of negative scattering density and only a few cycles are needed for this to happen. If convergence is reached during the application of the basic algorithm, these few cycles by the band CF algorithm will finish the job, and convergence will be undoubtedly signified by a large drop in the R factor. Otherwise, the R factor might either stagnate at a higher level without convergence or the drop may follow later, but the latter means that it was really the band CF algorithm that solved the structure. In the plots, we see the occurrence of all three possibilities. So we can only accept that the structure was solved by the basic algorithm if the following first few cycles of band CF signify a large drop in the R factor, *i.e.* band CF must be used just as a probe of convergence. Now let us see some numbers characterizing the performance of the 'basic + band' CF combination. Again, the optimal choice of δ is shown in the rightmost plots. The success rate is 100% for both examples and the number of iterations spent for a solution is 65 and 75 for examples I and II, respectively. We have made additional tests by decreasing the number of basic cycles from 500 to 200 and observed the same large drop in the R factor. We have also followed single runs, switched to band CF right after the basic drop, and checked the isosurface plot of the resulting scattering densities. These studies confirmed that the structure was solved in all cases, as an illustration see Fig. 6. After the drop observed during the basic cycles, the positive part of the scattering density was already recognized, while the complete structure developed in a few cycles.

The summary of this section is the following. *Ab initio* structure determination by using neutron diffraction data can be done by the combination of 'basic + band' CF. The combined algorithm is so efficient that *ab initio* structure determination by using neutron diffraction data becomes no more difficult than the X-ray case. This is remarkable, if we take into account the larger number of atoms, the presence of negative scattering density and that the pure band CF algorithm experienced orders-of-magnitude more difficulty.

6. Traps

A quick look at the upper panel of Fig. 4 (example I, neutron data and band flipping) reveals a characteristic difference between the first two and the last series of runs. In the first two series of using smaller δ, one can discern a broad distribution of convergence times. In the last series with larger δ, the iteration either converges – and then more rapidly – or does not converge at all. These unsuccessful runs were further continued up to 100000 iteration cycles without observing convergence. In this stagnation period, the scattering density apparently did not move, it became a steady state, *i.e.* the iteration process fell in a *trap*. Similar traps were observed with both neutron and X-ray data and for both test structures. Like the true scattering density, the steady state (trap) density ρ, *cf.* equation (1), has a small support, it vanishes in a large region of the unit cell. Apart from this property, the traps observed in cases I and II are rather different. For test structure I, decomposition of the real-space function into positive and negative parts, $\rho(\mathbf{r}) = \rho_+(\mathbf{r}) - \rho_-(\mathbf{r})$, where $\rho_+ \geq 0$, $\rho_- \geq 0$ and $\rho_+(\mathbf{r})\rho_-(\mathbf{r}) = 0$, shows that the two parts are approximate mirror images of each other: $\rho_-(\mathbf{r}) \approx \rho_+(M\mathbf{r})$, where M is the mirror operation perpendicular to the monoclinic b axis. The true scattering density does not possess this symmetry. Instead, in both structures, there is a c glide plane, and for case II it is this symmetry element that shows up in the trap density but without the complete space-group symmetry. In the case of example I, the false symmetry also implies $F(0) \approx 0$ while, for example II, the total charge significantly differs from zero. [Recall that the iteration lets $F(0)$ evolve freely.]

Let us note that a low space filling is not an exclusive property of trap densities; it generally characterizes the stagnating scattering density after the initial transient period. (But the unit cell is emptier for the traps than for the true structure or other temporary densities.) Whether such a density proves to be a trap or after a period of stagnation there is a rapid transition to convergence depends on the random initial condition. The chaotic properties of the iteration process, mentioned in Oszlányi & Sütő (2004, 2005), certainly have to do with the alternatives between stagnation and falling in a trap. While the details are unclear to us, we believe we partially understand how the algorithm favours the appearance of densities of a low space filling. Combined with the observed structure-factor moduli, any set of phases satisfying the constraint $\varphi(-\mathbf{h}) = -\varphi(\mathbf{h})$ defines a real function. The scattering density among them is distinguished by the fact that its support occupies a small fraction, typically less than 10%, of the unit cell. In other words, this is a function that is (nearly) zero over an extended domain. Whatever the route to convergence, band CF can tell the scattering density from any other function satisfying the modulus constraint only *via* these *plateaus* of zero. To see this, consider an ideal case when the distribution of the scattering density on the grid, *cf.* Fig. 2, is a step function with a wide step at zero level. If δ is chosen to be smaller than the smallest non-vanishing pixel value, the scattering density is a fixed point of the band CF algorithm. In realistic finite-resolution scattering densities, there are always pixel values between $-\delta$ and $+\delta$ and only the densities larger

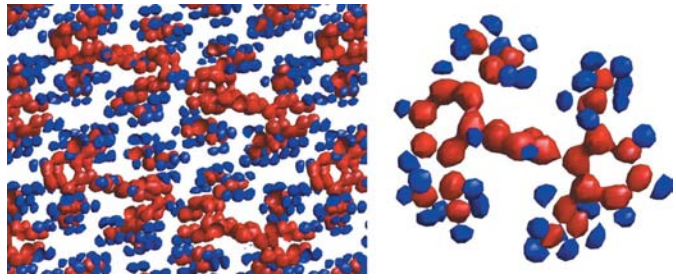

Figure 6
Reconstructed scattering density of the second test structure. Left and right panels show views of the crystal and a single molecule along the monoclinic b direction, while red and blue correspond to isosurface levels $+\delta$ and $-\delta$.

in modulus than $+\delta$ remain fixed after convergence, the values within the band vary in a two-cycle period. One might think that in the absence of homometric structures only the true scattering density and its translates, spatial and sign inverted pairs, exhibit the domain of zeros and are approximate fixed points of the iteration. However, one never encounters such fortunate cases.

Let $\rho(\mathbf{r})$ be the scattering density, and let $F(\mathbf{h})$ be its Fourier transform. Suppose that ρ can be written as $\rho_A + \rho_B$, where both components are real, have a plateau of zeros and the supports of their Fourier transforms F_A and F_B are disjoint: $F_A(\mathbf{h})F_B(\mathbf{h}) = 0$ for every $\mathbf{h}$. Then $\rho_A(\mathbf{r}) \pm \rho_B(\pm\mathbf{r} + \mathbf{a})$ is a real function that satisfies the modulus constraint and for most (if not all) translations $\mathbf{a}$ it will still present an extended domain of zeros in the overlap region of the respective plateaus of ρ_A and the translate of ρ_B. A realization of this scenario is as follows. Let

$$\rho_A(x, y, z) = \frac{1}{V}\sum_{h,k,l} F(2h, k, l)\exp[-2\pi i(2hx + ky + lz)] \quad (2)$$

and

$$\rho_B(x, y, z) = \frac{1}{V}\sum_{h,k,l} F(2h+1, k, l) \times \exp\{-2\pi i[(2h+1)x + ky + lz]\}. \quad (3)$$

Then

$$\begin{aligned} \rho_A\left(x+\tfrac{1}{2}, y, z\right) &= \rho_A(x, y, z) \\ \text{and} \qquad \rho_B\left(x+\tfrac{1}{2}, y, z\right) &= -\rho_B(x, y, z). \end{aligned} \quad (4)$$

Therefore,

$$\begin{aligned} \rho(x, y, z) &= \rho_A(x, y, z) + \rho_B(x, y, z) \\ \text{and} \quad \rho\left(x+\tfrac{1}{2}, y, z\right) &= \rho_A(x, y, z) - \rho_B(x, y, z), \end{aligned} \quad (5)$$

from which we obtain

$$\rho_A(x, y, z) = \tfrac{1}{2}\left[\rho(x, y, z) + \rho\left(x+\tfrac{1}{2}, y, z\right)\right] \quad (6)$$

$$\text{and} \quad \rho_B(x, y, z) = \tfrac{1}{2}\left[\rho(x, y, z) - \rho\left(x+\tfrac{1}{2}, y, z\right)\right]. \quad (7)$$

Typically, the plateaus of ρ and of its translate will overlap, thus both ρ_A and ρ_B will be real functions with zero plateau. Therefore, re-adding them with a relative shift, sign change and some symmetry element of the space group results in a false solution, a function with a plateau, typical for densities in the stagnation period. Other examples with shifts in two or three directions (or with the superposition of more than two shifted parts of the scattering density) can be constructed. Applying a shift by 0 or 1/2 in any of the three directions and combining the shifted function with the unshifted one according to equations (6), (7), we can obtain seven different pairs ρ_A, ρ_B. If the actual traps are really of the kind $\rho_A(\mathbf{r}) \pm \rho_B(\pm\mathbf{r} + \mathbf{a})$, one can understand that they occur more easily in the case of band flipping than with the original algorithm which forces positivity.

Finally, we want to stress two points. First, at least for test structure II, the most characteristic symmetry of the scattering density – the *c* glide plane – decided the kind of a trap that actually occurred. Second, the spatial stability of the trap density corresponds to a kind of phase locking. This may be a hint as to why the $\pi/2$ phase perturbation of weak reflections described in Oszlányi & Sütő (2005) helps to avoid the traps and increases the success rate of the CF algorithm.

7. Summary

In the present paper, we demonstrated that the charge flipping algorithm is able to solve structures using neutron diffraction data alone. We first discussed artificial and physical cases of negative scattering density, introduced a new version of the basic dual-space algorithm and selected some organic test structures with different hydrogen content. Band charge flipping reverses the sign of scattering density only within a zero-centred band and develops large plateaus without forcing positivity. Our tests showed that, while it works well, structure solution of neutron data with band flipping is orders-of-magnitude more difficult than structure solution of X-ray data with the basic algorithm. So we re-added the positivity constraint and experienced a significant speed up of convergence. The problem with such a solution is that it can be easily overlooked; by following the evolution of the *R* factor, the usual drop might be completely missing. Therefore, the band flipping algorithm must be used both as a probe of convergence and as a tool for developing negative densities. Only the 'basic + band' CF combination works reliably and fast, for our organic test structures the average number of iterations required by an X-ray and a neutron solution were similar.

This is a field that has both a long history and a promising future (Wilson, 2000). Starting in the early 1970's, it became clear that classical direct methods can be applied with success to neutron data (Sikka, 1969; Bernal & Watkins, 1972; Frey *et al.*, 1973; Hauptman & Langs, 2003). While the amount of negative scattering contribution is an important parameter of applicability, the real bottleneck was experimental. Even high-intensity reactor sources required very large single crystals and time-consuming experiments, so neutron diffraction was used sparingly for accurate structural refinements and not as a first choice for *ab initio* determination of unknown structures. Future prospects of this field are bright and are mostly determined by new developments of spallation sources. Their high intensity and easy access should make neutron experiments faster, bring down the required single-crystal size to today's X-ray average, and make *ab initio* neutron crystallography a common practice. In this situation, new algorithms specifically designed for structure solution using neutron data alone should find their applications, especially if their working principle differs from that of classical methods. Charge flipping is one of the options.

Finally, the present study also led to an important by-product. We could identify the traps that occasionally block the iterative process, and gave a mathematical analysis of their possible origin. This result is a starting point of further research and might have relevance on how symmetry should be handled and how the size limit of solvability can be increased.

APPENDIX *A*

Here we define $\bar{x}_S$, the *number of iterations spent for a solution*. This is a single indicator of the difficulty an algorithm meets in solving a structure with a success rate less than 100%. We found it quite reliable even if it was computed by choosing the maximum allowed number of iterations relatively small.

The calculation of run statistics requires the following protocol. (i) Select N different random phase sets. $N = 100$ is a common choice. (ii) Set M, the maximum number of iteration cycles allowed for a single run. $M = 5000$ is the choice of this paper. (iii) If the R-factor drop is large enough, then the point of convergence can be detected and the iteration process can be stopped. For each successful run, determine x_i, the number of iteration cycles where convergence occurs. (iv) Count n, the number of runs that converge before the maximum number of allowed iteration cycles is reached. (v) The usual success rate is $\eta = n/N$ but its value is not used here.

With these numbers, we can define $\bar{x}_S$. For $0 \leq n \leq N$, it reads

$$\bar{x}_S = \frac{\sum' x_i + (N - n)M}{n}, \tag{8}$$

where the prime indicates that the sum is only over the n converged runs. In particular, if $n = 0$ then $\bar{x}_S = \infty$, and if $n = N$ then $\bar{x}_S = (\sum_1^N x_i)/N$ is the usual average. This formula expresses very directly the total number of iteration cycles spent for a single structure solution. In other words, $\bar{x}_S$ takes into account both the useful iteration cycles of converged runs and the wasted cycles of non-converged runs. If the distribution of the convergence times were exponential, thus, without memory, $\bar{x}_S$ would be the empirical mean value of the number of iteration cycles in single runs up to convergence. However, preliminary computations show that in the present case the distribution of convergence times follows a power law, so this number is nothing more than what its name says.

This research was supported by OTKA grants T043494 and 67980K.

References

Abrahams, J. P. & Leslie, A. W. G. (1996). *Acta Cryst.* D**52**, 30–42.

Arduengo, A. J., Krafczyk, R., Schmutzler, R., Craig, H. A., Goerlich, J. R., Marshall, W. J. & Unverzagt, M. (1999). *Tetrahedron*, **55**, 14523–14534.

Baerlocher, Ch., McCusker, L. B. & Palatinus, L. (2006). *Acta Cryst.* A**62**, S231.

Baerlocher, Ch., McCusker, L. B. & Palatinus, L. (2007). *Z. Kristallogr.* **222**, 47–53.

Becker, H. D., Hall, S. R., Skelton, B. W. & White, A. H. (1982). *Austral. J. Chem.* **35**, 2357–2365.

Bernal, I. & Watkins, S. F. (1972). *Science*, **1978**, 1282–1283.

Brigham, E. O. (1974). *The Fast Fourier Transform*. Englewood Cliffs, NJ: Prentice-Hall.

Burla, M. C., Caliandro, R., Camalli, M., Carrozzini, B., Cascarano, G. L., de Caro, L., Giacovazzo, C., Polidori, G. & Spagna, R. J. (2005). *J. Appl. Cryst.* **38**, 381–388.

Elser, V. (2003). *Acta Cryst.* A**59**, 201–209.

Fienup, J. R. (1982). *Appl. Opt.* **21**, 2758–2769.

Frey, M. N., Lehmann, M. S., Koetzle, T. F. & Hamilton, W. C. (1973). *Acta Cryst.* B**29**, 876–884.

Frigo, M. & Johnson, S. G. (1998). *Proc. ICASSP*, **3**, 1381–1384.

Gerchberg, R. W. & Saxton, W. O. (1972). *Optik (Stuttgart)*, **35**, 237–246.

Gilmore, C. J. (2000). *Acta Cryst.* D**56**, 1205–1214.

Hauptman, H. A. & Langs, D. A. (2003). *Acta Cryst.* A**59**, 250–254.

Karle, I. L., Flippen-Anderson, J., Sukumar, M. & Balaram, P. (1987). *Proc. Natl Acad. Sci. USA*, **84**, 5087–5091.

Katrych, S., Weber, Th., Kobas, M., Massüger, L., Palatinus, L., Chapuis, G. & Steurer, W. (2007). *J. Alloys Compd*. **428**, 164–172.

Marks, L. D. (1999). *Phys. Rev. B*, **60**, 2771–2780.

Miller, R., DeTitta, G. T., Jones, R., Langs, D. A., Weeks, C. M. & Hauptman, H. A. (1993). *Science*, **259**, 1430–1433.

Oszlányi, G. & Sütő, A. (2004). *Acta Cryst.* A**60**, 134–141.

Oszlányi, G. & Sütő, A. (2005). *Acta Cryst.* A**61**, 147–152.

Oszlányi, G., Sütő, A., Czugler, M. & Párkányi, L. (2006). *J. Am. Chem. Soc.* **128**, 8392–8393.

Palatinus, L. (2004). *Acta Cryst.* A**60**, 604–610.

Palatinus, L., Dusek, M., Glaum, R. & Bali, B. E. (2006). *Acta Cryst.* B**62**, 556–566.

Sheldrick, G. M. (1997). *SHELXS97*, University of Göttingen, Germany.

Shiono, M. & Woolfson, M. M. (1992). *Acta Cryst.* A**48**, 451–456.

Sikka, S. K. (1969). Thesis, Bombay University, India.

Szöke, A. (1993). *Acta Cryst.* A**49**, 853–866.

Szöke, H. (2006). *EDEN User Manual, Version 5.3*, http://www.edencrystallography.org.

Wang, B. C. (1985). *Diffraction Methods for Biological Macromolecules*, Vol. 115, edited by H. W. Wyckoff, C. H. W. Hirs & S. N. Timasheff, pp. 90–113. Orlando, FL: Academic Press.

Wilson, C. C. (2000). *Single Crystal Neutron Diffraction from Molecular Materials*. Singapore: World Scientific.

Wu, J. S., Leinenweber, K., Spence J. C. H. & O'Keeffe, M. (2006). *Nature (Mater.)* **5**, 647–652.

Wu, J. S., Spence J. C. H., O'Keeffe, M. & Groy, T. L. (2004). *Acta Cryst.* A**60**, 326–330.

Zhang, K. Y. J., Cowtan, K. D. & Main, P. (2001). *International Tables for Crystallography*, Vol. F, edited by M. G. Rossmann & E. Arnold, pp. 311–324. Dordrecht: Kluwer.

Zúñiga, F. J., Palatinus, L., Cabildo, P., Claramunt, R. M. & Elguero, J. (2006). *Z. Kristallogr.* **221**, 281–287.